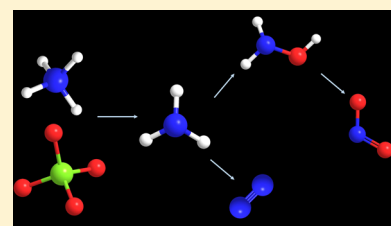


Electron Radiolysis of Ammonium Perchlorate: A Reflectron Time-of-Flight Mass Spectrometric Study

Sándor Góbi,^{†,‡} Alexandre Bergantini,^{†,‡} Andrew M. Turner,^{†,‡} and Ralf I. Kaiser^{*,†,‡,§}[†]Department of Chemistry and [‡]W. M. Keck Laboratory in Astrochemistry, University of Hawaii at Mānoa, Honolulu, Hawaii 96822, United States

Supporting Information

ABSTRACT: Thin films of ammonium perchlorate (NH_4ClO_4) were exposed to energetic electrons at 5.5 K to explore the radiolytic decomposition mechanisms. The effects of radiolysis were monitored on line and in situ via Fourier transform infrared spectroscopy (FTIR) in the condensed phase along with electron impact ionization quadrupole mass spectrometry (EI-QMS) and single-photon photoionization reflectron time-of-flight mass spectrometry (PI-ReTOF-MS) during the temperature-programmed desorption (TPD) phase to probe the subliming molecules. Three classes of molecules were observed: (i) nitrogen bearing species [ammonia (NH_3), hydroxylamine (NH_2OH), molecular nitrogen (N_2), nitrogen dioxide (NO_2)], (ii) chlorine carrying molecules [chlorine monoxide (ClO), chlorine dioxide (ClO_2), dichlorine trioxide (Cl_2O_3)], and (iii) molecular oxygen (O_2). Decay profiles of the reactants along with the growth profiles of the products as derived from the infrared data were fit kinetically to obtain a reaction mechanism with the initial steps involving a proton loss from the ammonium ion (NH_4^+) yielding ammonia (NH_3) and the decomposition of perchlorate ion (ClO_4^-) forming chlorate ion (ClO_3^-) plus atomic oxygen. The latter oxidized ammonia to hydroxylamine and ultimately to nitrogen dioxide. Molecular oxygen and nitrogen were found to be formed via recombination of atomic oxygen and multistep radiolysis of ammonia, respectively.



1. INTRODUCTION

Unraveling the decomposition mechanisms of solid rocket propellants such as of ammonium perchlorate (NH_4ClO_4) has been the focus of interest from the chemistry and materials science communities for the last half-century.¹ The first results on the thermal degradation of ammonium perchlorate were presented by Bircumshaw and Newman,² Jacobs and Whitehead,³ and Keenan and Siegmund.⁴ Ammonium perchlorate (NH_4ClO_4) was found to exhibit distinct decomposition mechanisms at “low” (below 240 °C) and “high” (above 350 °C) temperatures;^{1,5,6} the effects of the presence of catalysts such as metal oxides⁵ and of pressure⁷ were also examined. These studies concluded that the first decomposition step upon thermal degradation is a proton transfer from the ammonium cation (NH_4^+) expectedly to the perchlorate (ClO_4^-) counterion yielding ammonia (NH_3) (R1).¹



These investigations exploited mass spectrometry (MS),⁸ scanning electron microscopy (SEM),⁹ thermogravimetric analysis (TGA), and differential scanning calorimetry (DSC),¹⁰ as well as Raman spectroscopy.¹¹ The continuous advancement of analytical tools allowed for simultaneous detection techniques of the decomposition products within the same machine: TGA, SEM, DSC, and quadrupole MS (QMS)^{12,13} together with temperature-jump Fourier transform infrared spectroscopy (T-jump FTIR)¹⁴ and even TGA-FTIR/MS¹⁵ or TGA/DSC-FTIR/MS.¹⁶ A shock-wave-induced decomposition study of ammonium perchlorate

(NH_4ClO_4) was also performed.¹⁷ Attempts were also made to shed light on the effect of irradiation on the thermal decomposition of ammonium perchlorate with energetic particles; these experiments applied primarily X-ray, γ -rays,^{18,19} and neutrons.²⁰ Differential thermal analysis (DTA) and TGA methods were used predominantly; more recently, Dedgaonkar and Sarwade utilized the FTIR technique.²¹ Ivanov et al. exploited broadband ultraviolet (UV) light to produce dislocations and radiolysis products such as chlorate ions (ClO_3^-) that may alter the mechanism(s) of the low-temperature decomposition of ammonium perchlorate (NH_4ClO_4).^{22,23}

Contrary to the thermal degradation experiments, much less attention has been paid to the radiolytic decomposition of ammonium perchlorate (NH_4ClO_4) that could also explain why it affects its thermal degradation; these works mainly exploited γ - and X-ray irradiation as summarized in Table 1. The earliest studies utilized X-rays to irradiate ammonium perchlorate samples and monitored the formation of radicals via electron paramagnetic resonance (EPR).^{24,25} Both studies concluded that the ammoniumyl radical (NH_3^+) could be detected; this finding was later confirmed by Hegde et al. along with the observation of the chlorine trioxide (ClO_3) and chlorine dioxide (ClO_2) radicals.²⁶ Experiments using EPR after γ (and neutron) irradiation have also been performed.^{27,28} Besides

Received: February 25, 2017

Revised: April 26, 2017

Published: April 26, 2017

Table 1. Previous Experimental Results on the Radiolysis of Ammonium Perchlorate

sample	<i>p</i> (mbar)	<i>T</i> (K)	type of radiation, dose absorbed (eV/molecule)	detection	products	ref
single crystal	N/A	4.2, 300	X-ray, N/A	EPR	NH ₃ ⁺ radical	24
single crystal	N/A	93–373	X-ray, 4.9 × 10 ⁻²	EPR	NH ₃ ⁺ radical	25
single crystal	1013	283–288	γ (⁶⁰ Co source), 1.5	chemical analysis of products dissolved in water	Cl ⁻ , Cl ₂ , ClO ₃ ⁻ , OCl ⁻	30
single crystal	≈10 ⁻⁷	300	UV at 253.7 nm, N/A	UV-vis, EL-ReTOF-MS	absorption bands at 610, 360, and 295 nm, 610 nm band attributed to free electrons	31
single crystal	N/A	77–300	γ (⁶⁰ Co source), ≈1.2 × 10 ⁻²	EPR	no gaseous products in the MS spectrum	27
single crystal	N/A	77, 300	γ (⁶⁰ Co source), n ⁰ radiation, ≈4.2 × 10 ⁻² for both	EPR	NH ₃ ⁺ radical	28
single crystal	≈10 ⁻⁶	77	X-ray, UV at 253.7 nm, e ⁻ (1–12 MeV), 1.2 × 10 ⁻²	thermoluminescence (TL, 80–420 K), UV-vis	ClO ₃ , ClO ₂ , and NH ₃ ⁺ radicals	40
KBr pellets, microcrystalline	N/A	N/A	γ (⁶⁰ Co source), ≈6.1 × 10 ⁻¹	FTIR, UV-vis-NIR	TL peaks at 95, 113, 134, 246, 320 K, peak at 246 K attributed to ClO ₃ ⁻	29
single crystal	N/A	N/A	LIBS (Nd:YAG, 1064 nm), N/A	X-ray photoelectron spectroscopy; optical microscopy, SEM, AFM	UV-vis: 610 nm band attributed to F-centers, 300 nm to overlapping ClO ⁻ , ClO ₂ ⁻ , ClO ₃ ⁻ bands	32
single crystal	N/A	4.2, 77, 300	X-ray, N/A	EPR	cracking and “chemical decomposition” of sample	26
microcrystalline	air, Ar, N ₂ atmospheres	N/A	LIBS (Nd:YAG, 1064 nm), N/A	MIR and LWIR	NH ₃ ⁺ , ClO ₃ radical	33,
					parent ions NH ₄ ⁺ and ClO ₄ ⁻ exclusively	34

EPR, FTIR²⁹ and chemical analysis³⁰ of γ -radiolyzed samples were also carried out searching for chlorine trioxide (ClO_3), chlorate (ClO_3^-), chlorine dioxide (ClO_2), chlorite (ClO_2^-), hypochlorite (OCl^-), dichlorine molecule (Cl_2), chloride (Cl^-), nitrate (NO_3^-), and nitrite (NO_2^-). Only (in decreasing concentration) chloride (Cl^-), chlorine (Cl_2), chlorate (ClO_3^-), and hypochlorite (OCl^-) could be detected. Alternative radiation sources were rarely applied; irradiations by UV photons with a wavelength of 253.7 nm (4.89 eV) were carried out by Maycock and Pai Verneker reporting the formation of “color centers” attributed to free electrons within the sample.³¹ Furthermore, laser-induced breakdown spectroscopy (LIBS) was also conducted on ammonium perchlorate crystals (NH_4ClO_4) revealing mechanical deformations and (micro)cracking as well as the radiolytic decomposition of the sample with chlorates (ClO_3^-) as primary product. For these, Nd:YAG lasers (1064 nm) were utilized; the irradiation products were detected by X-ray photoelectron spectroscopy, optical microscopy, SEM, and atomic force microscopy (AFM).³² Yang et al. used the same method to trace the mid- and long-wave IR (MIR and LWIR) emission spectra of the sample.^{33,34}

Besides the experimental work, theoretical studies on the thermodynamical and spectral properties of ammonium perchlorate (NH_4ClO_4) have also been applied. The first paper by Barber et al. used the ab initio SCF-MO method to calculate the ionization energy of the perchlorate unit (ClO_4^-),³⁵ followed by more exhaustive simulations as the computational capacity of computers increased with time. Politzer and Lane utilized density functional theory (DFT) to calculate the energetics of the gas-phase decomposition steps of ammonium perchlorate (NH_4ClO_4 , at the B3PW91/6-311+G(2df) level of theory),³⁶ whereas Zhu and Lin compared the theoretical results obtained for the decay both in gas phase and solution phase at the CCSD(T)/6-311+G(3df,2p) and B3LYP/6-311+G(3df,2p) levels.³⁷ Most importantly, the electronic levels, vibrational and thermodynamical properties, and absorption spectra of crystalline ammonium perchlorate were investigated by Zhu et al.; they also utilized the DFT method.³⁸ Later, degradation kinetics and mechanism of ammonium perchlorate (NH_4ClO_4) were studied for the first time by first-principles calculations by Zhu and Lin.³⁹ It was found that the first step during the thermal decomposition is the sublimation of the ammonium perchlorate (NH_4ClO_4) followed by the formation of ammonia (NH_3) and perchloric acid (HClO_4).^{36,37,39} Both species may then take part in consecutive decomposition steps; these processes lead possibly to various nitrogen oxides (N_xO_y , $x = 1-2$, $y = 1-2$), hydroxylamine (NH_2OH), and chlorine oxides (Cl_xO_y , $x = 1-2$, $y = 1-7$).³⁶

It is imperative to point out that, despite all the efforts made so far, none of the previous works aimed to study the radiolytic decomposition products of ammonium perchlorate in solid state comprehensively. Furthermore, only a single study attempted to explore the electron-induced decomposition at low temperature (77 K) utilizing electron energies varying between 1 and 12 MeV; these authors observed chlorate (ClO_3^-), chlorine dioxide (ClO_2), chlorite (ClO_2^-), hypochlorite (OCl^-), and electron centers.⁴⁰ However, no experimental attempt has been made since then to unravel the detailed decomposition mechanisms and kinetics of ammonium perchlorate (NH_4ClO_4) destruction upon irradiation with ionizing radiation that also has an effect on the thermal degradation processes. The goal of the present article is

to tackle this open issue exploiting state-of-the-art single-photon photoionization reflectron time-of-flight mass spectrometry (PI-ReTOF-MS) of the products formed in the radiolysis of ammonium perchlorate at temperatures of 5 K allowing for the first identification of the nascent radiolysis products on line and in situ. This method is also supplemented by FTIR and EI-QMS monitoring of the sample during the irradiation and in the temperature-programmed-desorption (TPD) phase as well as by kinetic studies that help elucidate the main decomposition pathways.

2. EXPERIMENTAL METHODS

The experiments were conducted in a contamination-free ultrahigh vacuum (UHV) stainless steel chamber that can be evacuated to a base pressure of a few 10^{-11} mbar using oil-free magnetically suspended turbomolecular pumps and dry scroll backing pumps.⁴¹⁻⁴³ A polished silver wafer is used as a substrate and is mounted on a coldfinger made of oxygen-free high conductivity copper (OFHC) with indium foil between them to ensure thermal conductivity. The coldfinger is cooled by a closed-cycle helium refrigerator (Sumitomo Heavy Industries, RDK-415E) while the temperature can be maintained by the help of a heater connected to a programmable temperature controller; the substrate can be cooled down to 5.5 ± 0.1 K. The entire setup is freely rotatable within the horizontal plane and translatable in the vertical axis via a UHV compatible bellows and a differentially pumped rotational feedthrough. A thin film of microcrystalline ammonium perchlorate (NH_4ClO_4 , Sigma-Aldrich, 99.5%) with a thickness of 1050 ± 60 nm (Table 2) was prepared

Table 2. Ammonium Perchlorate Sample Preparation and CASINO Simulations

	NH_4ClO_4
mass weighed (g)	0.0370 ± 0.0001
mass of solvent H_2O (g)	25.25 ± 0.01
volume of solution used (mL)	0.225 ± 0.005
average density of film (g cm^{-3})	1.95 ± 0.01
average thickness of sample (nm)	1050 ± 60
molar mass (g mol^{-1})	117.49
sample surface area (cm^2)	1.81 ± 0.10
number of molecules in sample ($\times 10^{18}$)	1.89 ± 0.99
angle of incidence (deg)	70
irradiated area (cm^2)	1.5 ± 0.3
irradiation time (s)	3600 ± 2
applied electron current (nA)	34.5 ± 2.5
number of electrons generated ($\times 10^{14}$)	7.75 ± 0.56
initial energy of electrons (keV)	5.00
average backscattered energy of electrons (keV)	3.52 ± 0.07
average transmitted energy of electrons (keV)	0.00 ± 0.00
fraction of backscattered electrons (%)	41.6 ± 2.9
fraction of transmitted electrons (%)	0.0 ± 0.0
simulated average penetration depth (nm)	170 ± 10
number of exposed molecules ($\times 10^{17}$)	2.53 ± 0.54
dose per molecule (eV)	10.8 ± 2.5

on the substrate utilizing the method established previously.⁴⁴ Briefly, 0.0370 ± 0.0001 g of pure ammonium perchlorate (NH_4ClO_4) was dissolved in 25.25 ± 0.01 g of water (H_2O , Fisher Chemical, HPLC grade), and then 0.225 ± 0.005 mL of the solution was transferred to the silver substrate; the solvent was then evaporated by heating the samples up to 323–333 K.

The average thickness of the sample could be calculated from the volume of the solution added onto the substrate, the concentration of the solution, the average density ($1.95 \pm 0.01 \text{ g cm}^{-3}$), and the area of the solid sample ($1.81 \pm 0.10 \text{ cm}^2$). The calculated thickness could also be confirmed by weighing the mass of the ammonium perchlorate film (NH_4ClO_4 , $0.0004 \pm 0.0001 \text{ g}$) and dividing it by the average density and area of the solid sample; both methods yielded thicknesses of $1050 \pm 60 \text{ nm}$. The sample was then inserted into the main chamber. After evacuation, the complete system was pumped and baked for 2 days to eliminate residual gas contaminants. It should be noted that the temperature of sample was monitored throughout the bakeout, and it never exceeded 320 K ensuring that none of the sample material was lost. FTIR spectra were also taken before and after bakeout, confirming that the sample remained unchanged during this process. The sample was then cooled to $5.5 \pm 0.1 \text{ K}$ and was exposed isothermally to 5 keV electrons for 1 h at a current of $34.5 \pm 2.5 \text{ nA}$ over an area of $1.5 \pm 0.3 \text{ cm}^2$ at an angle of incidence of 70° relative to the surface normal (Table 2). It is worth noting that the experiment at this low temperature serves as a proof-of-concept study to shed light on the radiolytic decay mechanism of ammonium perchlorate (NH_4ClO_4) and on the formation pathways of volatile irradiation products.

The electron current was measured before and after the irradiation utilizing a Faraday cup (Kimball Physics, FC-71) mounted inside the main chamber. The number of electrons hitting the sample could then be calculated based on the average electron currents, and it was found to be $(7.75 \pm 0.56) \times 10^{14}$ electrons. Monte Carlo simulations utilizing CASINO software⁴⁵ were also performed to determine the dose absorbed ($10.8 \pm 2.5 \text{ eV}$ per ammonium perchlorate unit). It should be pointed out that the simulated average penetration depth of electrons ($170 \pm 10 \text{ nm}$) is significantly lower than the thickness of the sample ($1050 \pm 60 \text{ nm}$). This shows that the electrons interacted with the ammonium perchlorate (NH_4ClO_4) sample only, and not with the silver substrate itself.

The electron radiolysis of the sample was monitored online and in situ with the help of an FTIR spectrometer (Nicolet 6700) in the range $4000\text{--}650 \text{ cm}^{-1}$ at a resolution of 4 cm^{-1} . Each FTIR spectrum was collected for 2 min, resulting in a set of 30 infrared spectra during sample irradiation. The integrated band areas for the vibrational modes of the parent and of the products were then determined, and the number of molecules were calculated for every FTIR spectrum taken. Decay kinetics of the parent species as well as the growth profiles of radiolysis products were then numerically solved by assuming a set of coupled differential equations reflecting the decomposition and formation mechanisms.^{46–49} An electron ionization QMS (EI-QMS, Extrel Model 5221, in the mass range $1\text{--}100 \text{ m/z}$, with the electron impact energy of 70 eV ; at the filament current of 2 mA) operating in residual gas analyzer (RGA) mode was also utilized to probe the species sublimed into the gas phase. After irradiation, the sample was kept at $5.5 \pm 0.1 \text{ K}$ for an additional 1 h , and then a TPD study was performed by gradually warming the sample to 300 K at a rate of 1.0 K min^{-1} . Once it reached 300 K the sample was kept at this temperature for an additional 3 h to ensure that all volatile radiolysis product molecules sublimed into the gas phase. The subliming molecules were monitored using a reflectron time-of-flight mass spectrometer (PI-ReTOF-MS; Jordan TOF Products Inc.) by ionizing the subliming species via single photon ionization with coherent vacuum ultraviolet (VUV) light.^{41–43}

Pulsed VUV light at an energy of 10.82 eV (114.6 nm) was generated by nonlinear four wave mixing utilizing xenon (Xe) gas as the nonlinear medium⁵⁰ with about 10^{14} photons per pulse at a repetition rate of 30 Hz .⁴² A blank experiment (an identical one without electron irradiation) was also carried out to monitor potential contaminants.

3. RESULTS

3.1. Infrared Spectrum of Ammonium Perchlorate.

The FTIR spectra in the region $4000\text{--}650 \text{ cm}^{-1}$ of the ammonium perchlorate (NH_4ClO_4) sample collected before and during irradiation can be seen in Figure 1; the absorption

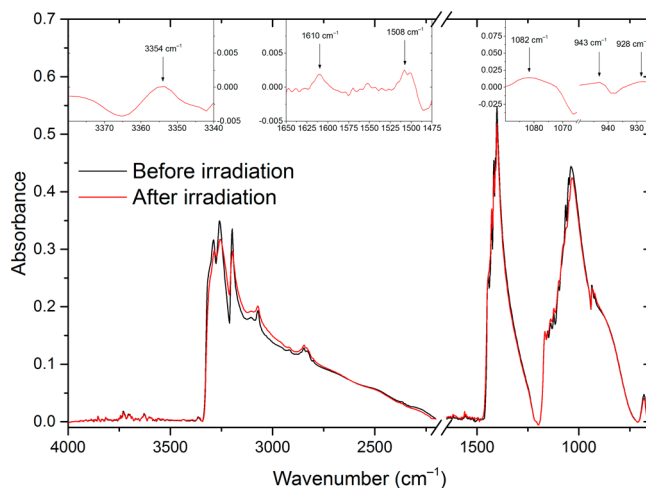


Figure 1. Infrared spectrum of NH_4ClO_4 sample before (black line) and after irradiation (red line). The insets show the difference spectra of the respective infrared regions with the arrows defining the position of the newly formed bands.

features are summarized in Table 3. The well-known infrared absorption features of the parent ions can clearly be detected;^{51–53} for instance, the antisymmetric and symmetric stretching vibrations of the ammonium ion ($\nu_{\text{as}} \text{NH}_4^+$ and $\nu_{\text{s}} \text{NH}_4^+$) are clearly visible at 3300 and 3198 cm^{-1} . Furthermore, the combination band of the bending modes of the ammonium ion ($\beta_{\text{s}} \text{NH}_4^+ + \beta_{\text{as}} \text{NH}_4^+$) and the overtone of the antisymmetric bending mode ($2\beta_{\text{as}} \text{NH}_4^+$) are observable in the region $3125\text{--}2800 \text{ cm}^{-1}$. The fundamental of the bending mode ($\beta_{\text{as}} \text{NH}_4^+$) can be seen at $1475\text{--}1200 \text{ cm}^{-1}$, whereas the intense and broad feature of the stretching modes of the perchlorate anion ($\nu_{\text{as}} \text{ClO}_4^-$ and $\nu_{\text{s}} \text{ClO}_4^-$) ranges from 1200 to 725 cm^{-1} . The positions of these vibrational modes—at 1050 and 930 cm^{-1} —are in agreement with the findings of previous studies probing magnesium perchlorate hexahydrate ($\text{Mg}(\text{ClO}_4)_2 \cdot 6\text{H}_2\text{O}$).^{43,54}

Besides the ubiquitous decrease of the vibrational modes associated with the reactant ions, novel absorption peaks arose during the exposure to ionizing radiation owing to newly formed radiolysis products.^{43,54} It is worth noting that no change could be observed in the FTIR spectrum of the blank experiment. Along with their decrease in intensity, the absorption bands of the ammonium perchlorate (NH_4ClO_4) also broaden when irradiated. This phenomenon can be explained by the degradation of the microcrystalline structure (amorphization) that forms as a result of the sample preparation method.^{44,55} New features can be observed at 3354 cm^{-1} caused by the antisymmetric stretching vibration of

Table 3. Infrared Absorption Peaks and Their Assignments for the Ammonium Perchlorate Samples As Well As for the Irradiation Products^a

pre-irrad ^b	post-irrad ^b	change upon irradi ^c	mode ^d	assignment ^d	ref
–	3354vw	+	ν_3 (NH ₃)	ν_{as} NH ₃	56
3315sh, 3306sh, 3290vs, 3259vs	3315sh, 3306sh, 3285vs, 3256vs	–, b	ν_3 (NH ₄ ⁺)	ν_{as} NH ₄ ⁺	52, 53
3198vs	3196vs	–, b	ν_1 (NH ₄ ⁺)	ν_s NH ₄ ⁺	52, 53
3106w, 3072w	3103vw, 3072w	–, b	$\nu_2 + \nu_4$ (NH ₄ ⁺)	cb (β_s NH ₄ ⁺ + β_{as} NH ₄ ⁺)	52, 53
2919w, 2885vw, 2862sh, 2848m, 2833m, 2801w	2820vw, 2847m, 2835sh, 2803sh	–, b	$2\nu_4$ (NH ₄ ⁺)	overtone ($2\beta_{as}$ NH ₄ ⁺)	52, 53
–	1610vw	+	ν_3 (NO ₂)	ν_{as} NO ₂	57, 58
–	1508vw	+	ν_4 (NH ₂ OH)	β NOH	59, 60
1445s, 1437sh, 1429s, 1417vs, 1409sh, 1402vs	1444sh, 1436sh, 1428sh, 1418s, 1409sh, 1402vs	–, b	ν_4 (NH ₄ ⁺)	β_{as} NH ₄ ⁺	52, 53
1167sh, 1154sh, 1139sh, 1123sh, 1100sh, 1088sh, 1076sh, 1065sh, 1051s, 1039vs,	1167sh, 1153sh, 1139sh, 1123sh, 1098sh, 1076sh, 1063sh, 1049sh, 1033vs	–, b	ν_3 (ClO ₄ [–])	ν_{as} ClO ₄ [–]	52, 53
–	1082w	+	ν_3 (ClO ₃ [–])	ν_{as} ClO ₃ [–]	43, 54
–	943vw, 928vw	+	ν_1 (ClO ₃ [–])	ν_s ClO ₃ [–]	43, 54
936w, 923w	936vw	–, b	ν_1 (ClO ₄ [–])	ν_s ClO ₄ [–]	52, 53

^aRadiolysis products are highlighted in bold. ^bWavenumbers in cm^{–1}: vs, very strong; s, strong; m, medium; w, weak; vw, very weak; sh, shoulder; b, broad; –, no signal. ^c–/+, decrease/increase of signal; b, broadening upon irradiation. ^dType of vibrational modes: ν , stretching; β , bending (scissoring); ρ , rocking; ω , wagging; τ , torsional; s, symmetric; as, antisymmetric; cb, combinational band.

the ammonia molecule (ν_{as} NH₃),⁵⁶ at 1610 cm^{–1} belonging to the antisymmetric stretching vibration of the nitrogen dioxide (ν_{as} NO₂),^{57,58} and at 1508 cm^{–1} belonging to the bending mode of hydroxylamine (NH₂OH) (β NOH).^{59,60} Additional new peaks can be found in the region dominated by the stretching vibration of the perchlorate unit (ClO₄[–]); these can be attributed to its decomposition product chlorate (ClO₃[–]). It should be noted that chlorites (ClO₂[–]) and chlorine dioxide (ClO₂) could not be attributed unambiguously.^{43,54} Here, the antisymmetric stretching vibration lies close to 1082 cm^{–1}, whereas the corresponding symmetric mode should be present at 943 and 928 cm^{–1} (Figure 1).

3.2. TPD Profiles of the Ammonium Perchlorate Samples. After irradiation, the EI-QMS and PI-ReTOF-MS TPD profiles of the samples were collected; these can be seen in Figures 2, 3, and 4, respectively. Radiolysis products can evidently be observed via EI-QMS (Figure 2a) with signal detectable at mass-to-ratios (m/z) of 28 (black), 30 (blue), 32 (red), and 46 (dark yellow). These belong to ions of molecular nitrogen (N₂⁺), nitrogen monoxide (NO⁺), molecular oxygen (O₂⁺), and nitrogen dioxide (NO₂⁺), respectively. These species depict multiple sublimation events; the first one starts at 160 K with a maximum at about 175 K, whereas the second, broader sublimation event starts at nearly 230 K with maxima at 260 and 290 K. The shape and position of the signal associated with molecular oxygen (O₂, m/z = 32) correlate well with previous radiolysis studies of perchlorate (ClO₄[–]) samples.⁴³ Here, the first peak can be linked to the in situ formation of molecular oxygen during the irradiation of perchlorates (ClO₄[–]), whereas the second peak might be related to the thermal degradation of higher chlorine oxides (Cl_xO_y, x = 1–2, y = 3–7) formed as byproducts upon irradiation. Alternatively, the molecules subliming from the upper, irradiated and therefore amorphized layer may account for the first

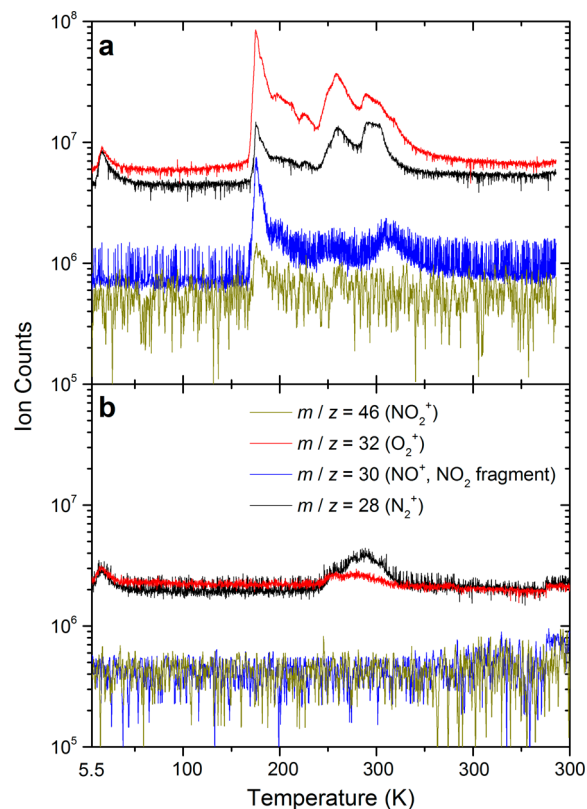


Figure 2. EI-QMS TPD profiles of molecules subliming from the irradiated ammonium perchlorate sample (a): m/z = 46 (NO₂⁺, dark yellow), m/z = 32 (O₂⁺, red), m/z = 30 (NO⁺, fragment of NO₂, blue), and m/z = 28 (N₂⁺, black). (b) EI-QMS TPD profiles of the blank experiment.

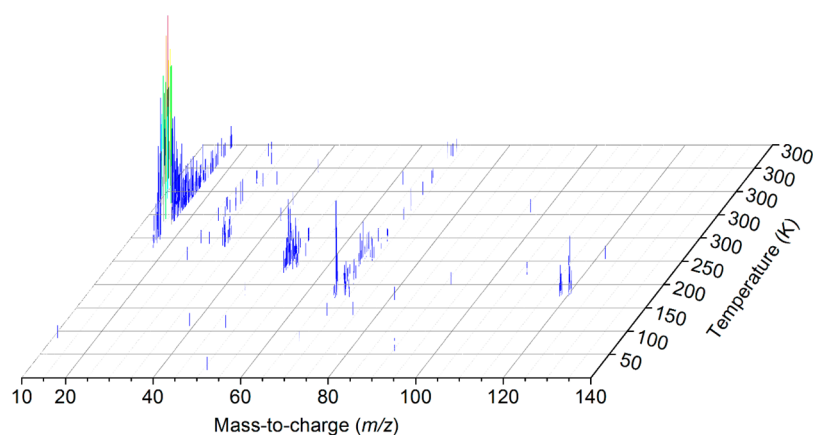


Figure 3. Three-dimensional visualization of PI-ReTOF-MS TPD of molecules subliming from the irradiated ammonium perchlorate sample from $m/z = 10$ to 140.

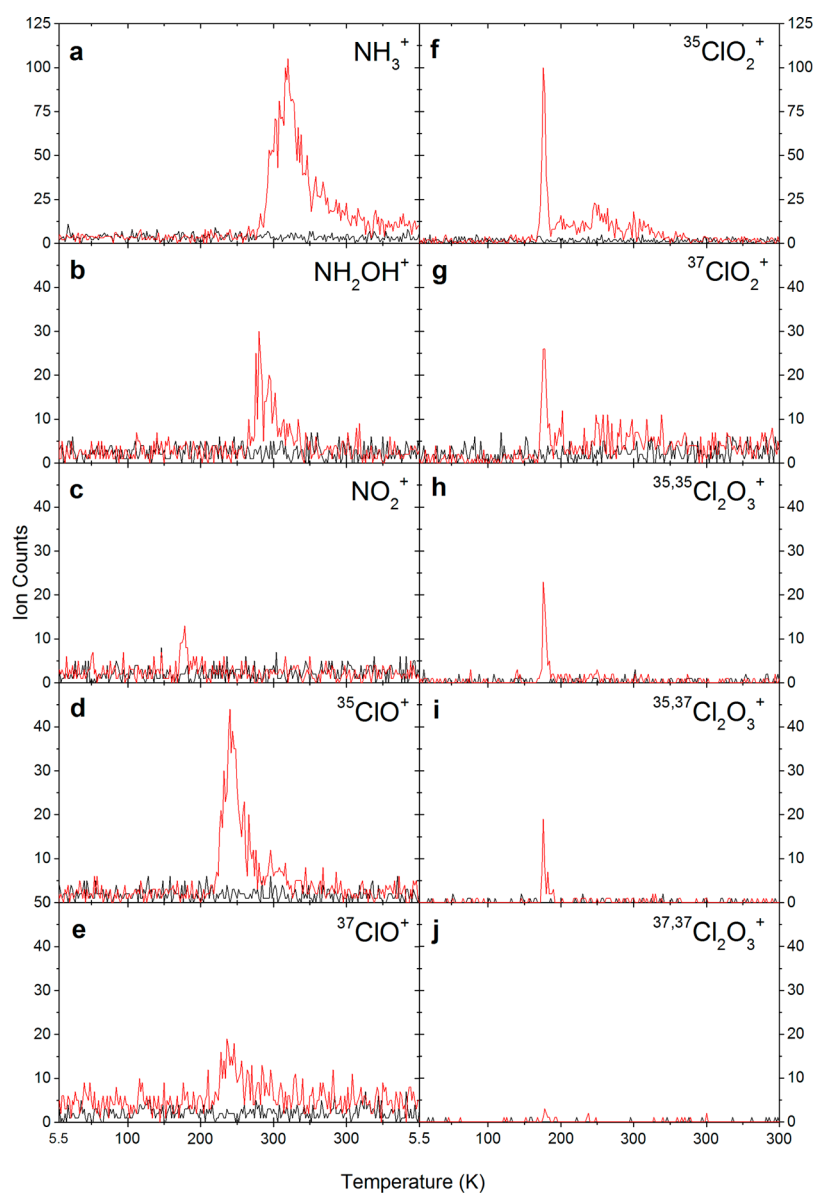


Figure 4. PI-ReTOF-MS TPD of molecules subliming from the irradiated ammonium perchlorate sample (red) and for the blank experiment (black): (a) $m/z = 17$ (NH_3^+), (b) $m/z = 33$ (NH_2OH^+), (c) $m/z = 46$ (NO_2^+), (d) $m/z = 51$ ($^{35}\text{ClO}^+$), (e) $m/z = 53$ ($^{37}\text{ClO}^+$), (f) $m/z = 67$ ($^{35}\text{ClO}_2^+$), (g) $m/z = 69$ ($^{37}\text{ClO}_2^+$), (h) $m/z = 118$ ($^{35,35}\text{Cl}_2\text{O}_3^+$), (i) $m/z = 120$ ($^{35,37}\text{Cl}_2\text{O}_3^+$), and (j) $m/z = 122$ ($^{37,37}\text{Cl}_2\text{O}_3^+$).

Table 4. Number of Radiolysis Product Molecules in the Irradiated Ammonium Perchlorate Samples Determined by FTIR, PI-ReTOF-MS, and EI-QMS

species	FTIR ^a	EI-QMS ^b	EI-QMS corrected ^{b,c}	PI-ReTOF-MS ^b	PI-ReTOF-MS corrected ^{b,d}	no. molecules based on EI-QMS or PI-ReTOF-MS ^e
NO ₂	$(3.41 \pm 0.31) \times 10^{14}$	$(6.89 \pm 0.96) \times 10^{7f}/$ $(1.89 \pm 0.17) \times 10^{8g}$	$(1.63 \pm 0.16) \times 10^{8h}$	122	2665	$(3.57 \pm 0.01) \times 10^{14}$
NH ₂ OH	$(1.25 \pm 0.06) \times 10^{16}$	–	–	793	N/A	–
NH ₃	$(8.30 \pm 0.03) \times 10^{14}$	–	–	6192	6192	$(8.30 \pm 0.03) \times 10^{14}$
O ₂	–	$(2.97 \pm 0.25) \times 10^9$	$(2.97 \pm 0.25) \times 10^9$	–	–	$(6.21 \pm 1.67) \times 10^{15}$
N ₂	–	$(9.86 \pm 0.67) \times 10^8$	$(7.25 \pm 0.49) \times 10^8$	–	–	$(1.55 \pm 0.37) \times 10^{15}$
ClO ₃ [–]	+	–	–	–	–	–
ClO ₂	–	–	–	2359/860 ⁱ	4747/1730 ⁱ	$(6.74 \pm 0.37) \times 10^{14}$
Cl ₂ O ₃	–	–	–	148/102/16 ⁱ	332/228/36 ⁱ	$(4.51 \pm 0.11) \times 10^{13}$
ClO	–	–	–	1536/610 ⁱ	3441/1366 ⁱ	$(5.10 \pm 0.48) \times 10^{14}$

^aNumber of molecules determined by using the integrated infrared absorption coefficients. +, Detection without quantification; –, could not be detected by the respective method. ^bIntegrated ion counts; –, could not be detected by the respective method. ^cCorrected for the electron ionization cross section of O₂ at electron energy of 70 eV. ^dCorrected for the photoionization cross section of NH₃ at photon energy of 10.82 eV. ^eNumber of molecules determined by using the PI-ReTOF-MS results; the italicized values for O₂ and N₂ were done by using the EI-QMS signals. ^fValue obtained for $m/z = 46$ (NO₂⁺). ^gValue obtained for $m/z = 30$ (NO⁺, NO₂ fragment). ^hAveraged value of $m/z = 46$ (NO₂⁺) and $m/z = 30$ (NO⁺, NO₂ fragment). ⁱThe values represent the ion counts of the respective isotopologues.

sublimation peak, while the second broad peak can be due to molecules that diffused to deeper, intact layers of the sample at the early stages of the TPD and sublime from there at higher temperatures. The fact that the nitrogen molecule (N₂) could not be detected via FTIR can be explained by the extremely small IR absorption coefficient of the stretching vibration of N₂ at 2328 cm^{–1} in a polar matrix being only 1.8×10^{-22} cm molecule^{–1}.⁶¹ The same holds true for the oxygen molecule (O₂) that has an absorption coefficient of 5×10^{-21} cm molecule^{–1} for its stretching vibration at 1550 cm^{–1}.⁶² The nitrogen monoxide (NO⁺) ions can be associated with the electron impact fragmentation of nitrogen dioxide (NO₂) at electron ionization energies of 70 eV,⁶³ which is justified by the fact that the stretching fundamental of nitrogen monoxide (NO) cannot be observed in the FTIR spectrum.

The TPD profiles taken by the PI-ReTOF-MS instrument also reveal strong evidence of distinct radiolysis products (Figures 3 and 4). These are peaks at $m/z = 17, 33, 46, 51/53, 67/69,$ and $118/120/122$. These ion counts can be correlated with the formation of ammonia (NH₃⁺, Figure 4a, ionization energy (IE) = 10.069 ± 0.002 eV),⁶⁴ hydroxylamine (NH₂OH⁺, Figure 4b, IE = 10.0 eV),⁶⁵ nitrogen dioxide (NO₂⁺, Figure 4c, IE = 9.75 ± 0.01 eV),⁶⁶ chlorine monoxide (³⁵ClO⁺ and ³⁷ClO⁺, Figure 4d,e, IE = 10.85 ± 0.05 eV),⁶⁷ chlorine dioxide (³⁵ClO₂⁺ and ³⁷ClO₂⁺, Figure 4f,g, IE = 10.33 ± 0.02 eV),⁶⁸ and dichlorine trioxide (³⁵Cl₂O₃⁺, ^{35,37}Cl₂O₃⁺, ³⁷Cl₂O₃⁺, Figure 4h–j, IE = 11.11 ± 0.02 eV, theoretical value).⁶⁹ The fact that no nitrogen monoxide (NO) was observed supports the conclusion that the ion counts at $m/z = 30$ in the EI-QMS detection originate from dissociative ionization of nitrogen dioxide (NO₂, Figure 2a). Chlorine dioxide (ClO₂) could also be detected in previous perchlorate (ClO₄[–]) irradiation experiments, where it was found that the integrated ion counts reflect well the chlorine isotope natural abundance ratio: ³⁷Cl:³⁵Cl = 0.327:1.000 vs $I[^{37}\text{ClO}_2]:I[^{37}\text{ClO}_2] = 0.342 \pm 0.024$;⁴³ whereas the same value for chlorine monoxide is $I[^{37}\text{ClO}]:I[^{37}\text{ClO}] = 0.397 \pm 0.028$. The ratio of integrated ion counts of dichlorine trioxide (Cl₂O₃) isotopologues at $m/z = 118, 120,$ and 122 is obtained to be $I[^{35,35}\text{Cl}_2\text{O}_3]:I[^{35,37}\text{Cl}_2\text{O}_3]:I[^{37,37}\text{Cl}_2\text{O}_3] = 1:0.689:0.108$, which compares well to the natural isotopic ratio of compounds containing two chlorine atoms (^{35,35}Cl₂:^{35,37}Cl₂:^{37,37}Cl₂ =

1.000:0.654:0.109). It is important to note that the signal of ^{37,37}Cl₂O₃ at $m/z = 122$ is barely higher than the background noise due to the low abundance of the isotopologue containing two ³⁷Cl atoms (Figure 4j). In contrast to EI-QMS (Figure 2), molecular nitrogen (N₂, $m/z = 28$) and oxygen (O₂, $m/z = 32$) could not be detected via PI-ReTOF-MS due to their high ionization energies (IE = 15.581 ± 0.008 and 12.0697 ± 0.0002 eV);^{70,71} the same holds true for chlorine oxides (Cl_xO_y, $x = 1–2, y = 1–7$) other than chlorine monoxide (ClO), chlorine dioxide (ClO₂), and dichlorine trioxide (Cl₂O₃).⁴³ Table 4 summarizes the radiolysis products and the methods of their detection. It is also important to note that although ammonia (NH₃) should be detectable via EI-QMS as well, its signal is masked by the ubiquitous signal of the water background (from atmospheric contamination) and its fragments ($m/z = 17; \text{OH}^+$).

4. DISCUSSION

4.1. Quantification of Radiolysis Products. The radiolysis products can be quantified by the FTIR method if their integrated absorption coefficients and band areas are known (Table 4).⁷² Based on the integrated absorption coefficient of the ammonia fundamental at 3354 cm^{–1} (3.11×10^{-17} cm molecule^{–1})⁷³ the number of ammonia (NH₃) molecules in the sample after the irradiation is computed to be $(8.30 \pm 0.03) \times 10^{14}$. The remaining molecules that can be quantified based on their infrared bands are nitrogen dioxide (NO₂, 6.36×10^{-17} cm molecule^{–1}; 1610 cm^{–1})⁵⁸ and hydroxylamine (NH₂OH, 4.16×10^{-18} cm molecule^{–1}, 1508 cm^{–1})⁷⁴ corresponding to $(3.41 \pm 0.31) \times 10^{14}$ and $(1.25 \pm 0.06) \times 10^{16}$ molecules after radiolysis, respectively.

It is also of primary importance to account for the remaining products such as nitrogen (N₂) and oxygen (O₂) as their intense signals in the EI-QMS spectrum (Figure 2a) suggest that they are both abundant species in the sample after irradiation. Although the current experiment cannot quantify them directly by infrared spectroscopy due to their very small integrated infrared absorption coefficients (section 3.2), their yields can be calculated via the background corrected, integrated ion counts and by accounting for their electron ionization cross sections. Namely, the integrated ion counts are found to be $(9.86 \pm 0.67) \times 10^8$ and $(2.97 \pm 0.25) \times 10^9$ for

molecular nitrogen (N_2) and oxygen (O_2), respectively (Table 4). Furthermore, the counts of the former can be corrected by the electron ionization cross section relative to molecular oxygen at 70 eV (1:1.36, Supporting Information); the corrected integrated EI-QMS signal is obtained to be $(7.25 \pm 0.49) \times 10^8$ (Table 4). Furthermore, the integrated EI-QMS signals of nitrogen dioxide (NO_2) for its molecular ion at $m/z = 46$ (NO_2^+) and for its fragment ion at $m/z = 30$ (NO^+) can be corrected with their relative electron impact ionization cross sections of 0.388 and 1.28 using molecular oxygen as the reference of 1.0; these values average to $(1.63 \pm 0.16) \times 10^8$ (Table 4). Defining these corrected counts from the EI-QMS data as $(3.41 \pm 0.31) \times 10^{14}$ molecules as obtained from FTIR, the ion counts of nitrogen and oxygen translate to the formation of $(1.55 \pm 0.37) \times 10^{15}$ and $(6.21 \pm 1.67) \times 10^{15}$ molecules, respectively,

Similarly, the value for the chlorine-bearing radiolysis products such as chlorine dioxide (ClO_2) cannot be determined directly due to their weak IR signals which are masked by the intense signal of the perchlorate unit (ClO_4^-) of the parent species. However, they can be calculated by a similar method applied for molecular oxygen (O_2) and nitrogen (N_2). Their integrated PI-ReTOF-MS ion counts can be corrected by their relative photoionization cross sections at the photoionization energy of 10.82 eV using ammonia (NH_3) as a reference (Table 4, Supporting Information). Then, if multiplied by the number of ammonia molecules in the sample, the values of $(6.74 \pm 0.37) \times 10^{14}$, $(5.10 \pm 0.48) \times 10^{14}$, and $(4.51 \pm 0.11) \times 10^{13}$ molecules can be obtained for the number of chlorine dioxide (ClO_2), chlorine monoxide (ClO), and chlorine trioxide (Cl_2O_3) molecules, respectively. It is important to note that the number of molecules calculated by using the corrected integrated PI-ReTOF-MS ion counts of the isotopologues of these chlorine compounds agree exceptionally well. Moreover, the use of this method is further justified by the fact that the ratio of the number of molecules for nitrogen dioxide (NO_2) to ammonia (NH_3) as determined by the FTIR method correlates well with that obtained via PI-ReTOF-MS: 0.41 ± 0.04 and 0.43 ± 0.03 , respectively.

The last species that can be detected is the chlorate anion (ClO_3^-), whose arising infrared signal can be clearly seen in Figure 1. Although its number in the sample cannot be calculated by any of the methods described above, an estimate can still be given by exploiting the number of nitrogen atoms needed for the formation of the products containing this element (NO_2 , NH_2OH , N_2 , NH_3 , $(1.68 \pm 0.14) \times 10^{16}$). This value should be identical to the number of decomposed ammonium perchlorate (NH_4ClO_4) units since every destroyed parent species yields only one nitrogen atom. Moreover, this should also be equal to the total chlorine atoms in the newly formed products; when this value is compared to the total number of chlorine atoms needed for the formation of chlorine dioxide (ClO_2), dichlorine trioxide (Cl_2O_3), and chlorine monoxide (ClO , $(1.27 \pm 0.09) \times 10^{15}$), it can be clearly seen that these species account only for $8 \pm 1\%$ of the total number of perchlorate units (ClO_4^-) decomposed. Chlorate (ClO_3^-) likely accounts for the rest of chlorine atoms according to earlier results.^{75,76} It is also imperative to point out that the total oxygen atoms formed is higher than the nitrogen atom incorporated into new products with oxygen atoms incorporated being $(2.56 \pm 0.40) \times 10^{16}$. Considering the ratio of oxygen to nitrogen to be 1.5 ± 0.3 , some of the perchlorate ions (ClO_4^-) must lose more than one oxygen atom during the

irradiation as is evident from the chlorine oxides formed. The ratio higher than 1 also requires that some of the perchlorate ions (ClO_4^-) are converted to chlorite ions (ClO_2^-) or other chlorine oxides rather than chlorate ions (ClO_3^-).

4.2. Decay Mechanism of Ammonium Perchlorate.

Based on the obtained FTIR, EI-QMS, and PI-ReTOF-MS data (sections 3.1 and 3.2), the following decay mechanism for the ammonium perchlorate (NH_4ClO_4) can be derived (Figure 5).

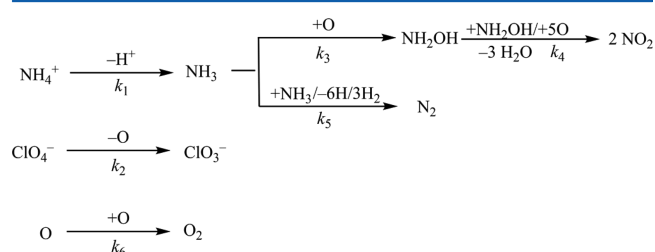


Figure 5. Reaction pathways in radiolyzed ammonium perchlorate.

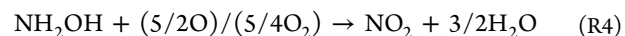
The temporal profiles of the decomposition products (hydroxylamine (NH_2OH), ammonia (NH_3), nitrogen dioxide (NO_2)) could be fit numerically with the reaction equations summarized in Table 5; the results are compiled in Figure 6. These findings propose that the first steps represent a deprotonation of the ammonium (NH_4^+) cation forming ammonia (NH_3) (R1).^{36,37,39} Also, the perchlorate unit (ClO_4^-) may lose an oxygen when exposed with energetic electrons, yielding the chlorate ion (ClO_3^-) (R2).^{43,54} The rate constants k_1 and k_2 are identical within error limits (Table 5).



The kinetic fits suggest that ammonia is consumed via oxidation forming hydroxylamine (NH_2OH) (R3); this pathway likely proceeds via insertion of atomic oxygen into a N–H bond of ammonia followed^{77,78} by intersystem crossing if the oxygen is in its triplet ground state. The barrier to insertion of 12.3 kJ mol^{-1} can be easily overcome by suprathreshold oxygen atoms produced in the decomposition of the perchlorate anion.⁷⁸



However, the temporal profile requires that hydroxylamine is being consumed as well. The growth profile of its terminal oxidation product nitrogen dioxide (NO_2) can be fit well by incorporating an overall multistep pathway (R4). This reaction can easily occur in a highly oxidizing environment.



Even with the oxidation to hydroxylamine, the ammonia (NH_3) temporal profile still requires a second loss pathway. Previous laboratory studies provided compelling evidence that molecular nitrogen (N_2) as detected via EI-QMS represents the terminal hydrogen loss product of ammonia. Here, Zheng et al. revealed that molecular nitrogen readily forms from ammonia via a Rice–Herzfeld chain as expressed via the net reaction (R5).^{79,80}



Table 5. Rate Constants (in s^{-1}) Based on the Kinetic Scheme As Compiled in Figure 5

reaction			
no.	equation	rate const	value
R1	$NH_4^+ \rightarrow NH_3 + H^+$	k_1	$(1.96 \pm 0.05) \times 10^{-4}$
R2	$ClO_4^- \rightarrow ClO_3^- + O$	k_2	$(1.83 \pm 0.14) \times 10^{-4}$
R3	$NH_3 + O \rightarrow NH_2OH$	k_3'	$(6.15 \pm 0.29) \times 10^{-3a}$
R4	$NH_2OH + (5/2O)/(5/4O_2) \rightarrow NO_2 + 3/2H_2O$	k_4'	$(7.24 \pm 0.29) \times 10^{-6a,b}$
R5	$2NH_3 \rightarrow N_2 + 3H_2/6H$	k_5'	$(9.41 \pm 0.83) \times 10^{-3a,b}$
R6	$O + O \rightarrow O_2$	k_6'	$(8.19 \pm 0.39) \times 10^{-3a}$

^aPseudo-first-order values of higher-order rates obtained by assuming the average number of oxygen atoms in the sample to be $n[O]_{av} = (1.38 \pm 0.70) \times 10^{15}$ according to the steady-state approximation. ^bNet equation of multiple reaction steps; reaction orders were determined empirically.

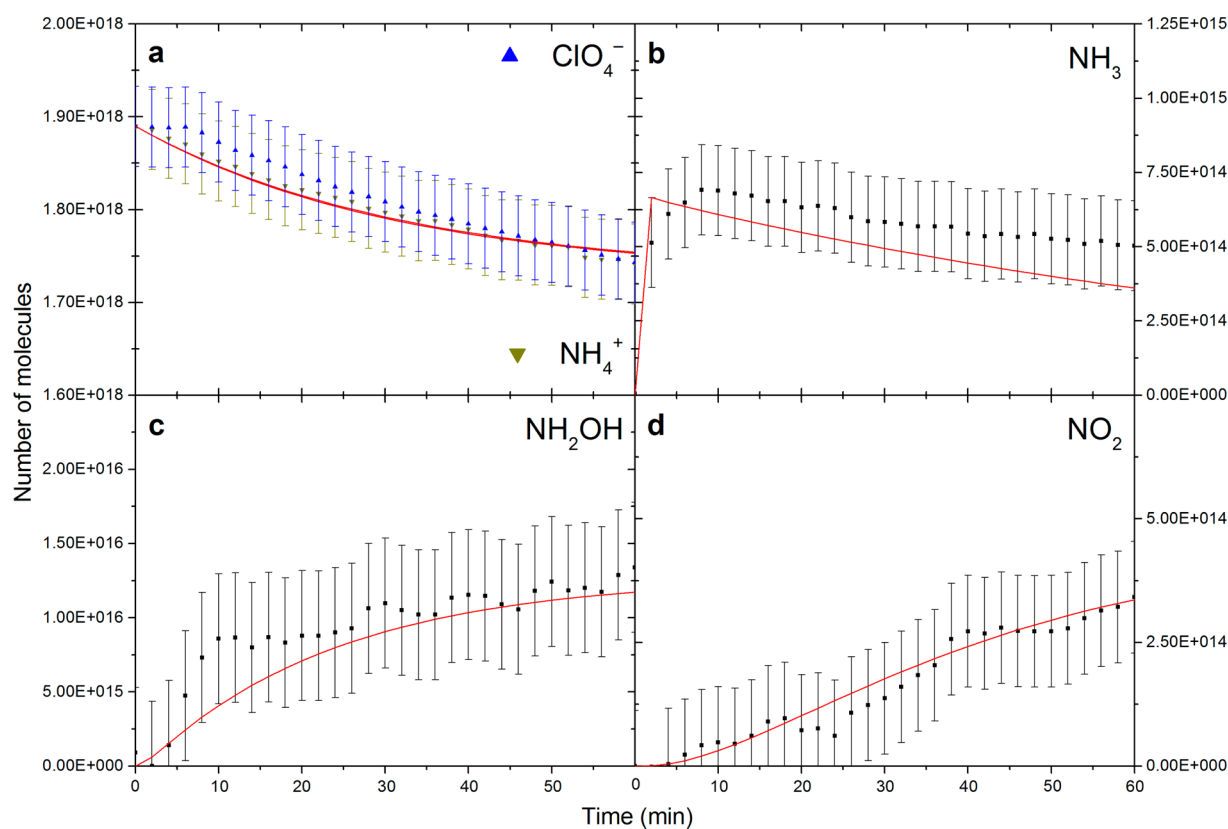


Figure 6. Experimental decay curves of IR bands (a) at 3198 cm^{-1} (ν_s NH_4^+ vibration of NH_4ClO_4 , dark yellow down-pointing triangle) and at $1250\text{--}750\text{ cm}^{-1}$ (ν_s and ν_{as} ClO_4^- vibration of NH_4ClO_4 , blue up-pointing triangle). Experimental growth curves of IR bands (b) at 3354 cm^{-1} (ν_{as} NH_3 vibration of the NH_3 molecule, black circle), (c) at 1508 cm^{-1} (β NOH vibration of the NH_2OH molecule, black circle), and (d) at 1610 cm^{-1} (ν_{as} NO_2 vibration of the NO_2 molecule, black circle) upon electron irradiation. Theoretical decay/growth curves obtained by numerically solving the coupled differential equations resulting from the reaction scheme in Figure 5: in (a)–(d) the lines overlaid in red.

Also, the unreacted atomic oxygen then recombines into molecular oxygen (O_2) (R6) and can be observed in the EI-QMS TPD profile upon its sublimation.^{43,54}



Note that chlorates (ClO_3^-) formed in reaction R2 presumably partly decompose further into chlorites (ClO_2^-) and/or chlorine dioxide (ClO_2) along with atomic oxygen,¹ which may also help in the oxidation of the irradiation products.⁴³ This reaction mechanism discussed above is strongly confirmed by the kinetic study of the decay/growth profiles of the reactants/products, which exploits the numerical solution of the coupled differential equations based on the reactions described in Table 5 (Figure 6).⁴⁶

5. CONCLUSION

In summary, thin films of ammonium perchlorate (NH_4ClO_4) were exposed to energetic electrons at 5.5 K to unravel the radiolytic decomposition mechanisms. The effects of radiolysis were monitored online and in situ via FTIR in the condensed phase along with EI-QMS and PI-ReTOF-MS methods during the TPD phase to probe the subliming molecules. In contrast to previous irradiation studies, this allowed for the detection of numerous different radiolysis products facilitating the determination of the decomposition pathways as well. Three classes of molecules were observed: (i) nitrogen bearing species [ammonia (NH_3), hydroxylamine (NH_2OH), nitrogen dioxide (NO_2), nitrogen (N_2)], (ii) chlorine carrying molecules [chlorine monoxide (ClO), chlorine dioxide (ClO_2), dichlorine trioxide (Cl_2O_3)], and (iii) molecular oxygen [O_2]. The decay

profiles of reactants along with the growth profiles of products as derived from the infrared data were fit kinetically to obtain a reaction mechanism with the initial steps involving a proton loss from the ammonium ion (NH_4^+) yielding ammonia (NH_3) and a decomposition of the perchlorate ion (ClO_4^-) forming the chlorate ion (ClO_3^-) plus atomic oxygen. The latter oxidized ammonia to hydroxylamine (NH_2OH) and ultimately to nitrogen dioxide (NO_2). Molecular oxygen (O_2) and nitrogen (N_2) were found to be formed via recombination of atomic oxygen and multistep radiolysis of ammonia via a Rice–Herzfeld chain, respectively. Based on the overall mass balance, the chlorine bearing compounds were synthesized when the chlorate ion (ClO_3^-) decomposed further into nascent oxygen and various chlorine oxides in lower oxidation states. This work represents the first comprehensive experimental examination of the effects of the radiolysis of ammonium perchlorate (NH_4ClO_4) aiming to untangle the decomposition mechanism of this important molecule used as a solid rocket propellant. It also serves as the first step of a set of experiments that continues in the understanding of the thermal degradation of the molecule that will be studied by utilizing a novel CO_2 laser apparatus in the near future.

■ ASSOCIATED CONTENT

Supporting Information

The Supporting Information is available free of charge on the ACS Publications website at DOI: 10.1021/acs.jpca.7b01862.

Absolute and relative electron ionization and photoionization cross sections of the species detected by EI-QMS and PI-ReTOF-MS methods (PDF)

■ AUTHOR INFORMATION

Corresponding Author

*E-mail: ralfk@hawaii.edu.

ORCID

Ralf I. Kaiser: 0000-0002-7233-7206

Notes

The authors declare no competing financial interest.

■ ACKNOWLEDGMENTS

This work was supported by the Office of Naval Research under Grant N00014-16-1-2078.

■ REFERENCES

- (1) Boldyrev, V. V. Thermal Decomposition of Ammonium Perchlorate. *Thermochim. Acta* **2006**, *443*, 1–36.
- (2) Bircumshaw, L. L.; Newman, B. H. The Thermal Decomposition of Ammonium Perchlorate. I. Introduction, Experimental, Analysis of Gaseous Products, And Thermal Decomposition Experiments. *Proc. R. Soc. London, Ser. A* **1954**, *227*, 115–132.
- (3) Jacobs, P. W. M.; Whitehead, H. M. Decomposition and Combustion of Ammonium Perchlorate. *Chem. Rev.* **1969**, *69*, 551–590.
- (4) Keenan, A. G.; Siegmund, R. F. Thermal Decomposition of Ammonium Perchlorate. *Q. Rev., Chem. Soc.* **1969**, *23*, 430–452.
- (5) Rosser, W. A.; Inami, S. H.; Wise, H. Thermal Decomposition of Ammonium Perchlorate. *Combust. Flame* **1968**, *12*, 427–435.
- (6) Jacobs, P. W. M.; Pearson, G. S. Mechanism of the Decomposition of Ammonium Perchlorate. *Combust. Flame* **1969**, *13*, 419–430.
- (7) Lang, A. J.; Vyazovkin, S. Effect of Pressure and Sample Type on Decomposition of Ammonium Perchlorate. *Combust. Flame* **2006**, *145*, 779–790.
- (8) Heath, G. A.; Majer, J. R. Mass Spectrometric Study of the Thermal Decomposition of Ammonium Perchlorate. *Trans. Faraday Soc.* **1964**, *60*, 1783–1791.
- (9) Boggs, T. L.; Kraeutle, K. J. Role of the Scanning Electron Microscope in the Study of Solid Rocket Propellant Combustion. I. Ammonium Perchlorate Decomposition and Deflagration. *Combust. Sci. Technol.* **1969**, *1*, 75–93.
- (10) Vyazovkin, S.; Wight, C. A. Kinetics of Thermal Decomposition of Cubic Ammonium Perchlorate. *Chem. Mater.* **1999**, *11*, 3386–3393.
- (11) Brill, T. B.; Goetz, F. Laser Raman Study of the Thermal Decomposition of Solid NH_4ClO_4 . *J. Chem. Phys.* **1976**, *65*, 1217–1219.
- (12) Majda, D.; Korobov, A.; Filek, U.; Sulikowski, B.; Midgley, P.; Vowles, D.; Klinowski, J. Low-Temperature Thermal Decomposition of Large Single Crystals of Ammonium Perchlorate. *Chem. Phys. Lett.* **2008**, *454*, 233–236.
- (13) Majda, D.; Korobov, A.; Filek, U.; Sulikowski, B.; Midgley, P.; Nicol, D. A.; Klinowski, J. Low-Temperature Thermal Decomposition of Crystalline Partly and Completely Deuterated Ammonium Perchlorate. *Chem. Phys. Lett.* **2011**, *504*, 185–188.
- (14) Brill, T. B.; Brush, P. J.; Patil, D. G. Thermal Decomposition of Energetic Materials 60. Major Reaction Stages of a Simulated Burning Surface of NH_4ClO_4 . *Combust. Flame* **1993**, *94*, 70–76.
- (15) Mallick, L.; Kumar, S.; Chowdhury, A. Thermal Decomposition of Ammonium Perchlorate—A TGA–FTIR–MS Study: Part I. *Thermochim. Acta* **2015**, *610*, 57–68.
- (16) Zhu, Y.-L.; Huang, H.; Ren, H.; Jiao, Q.-J. Kinetics of Thermal Decomposition of Ammonium Perchlorate by TG/DSC-MS-FTIR. *J. Energ. Mater.* **2014**, *32*, 16–26.
- (17) Gruzdkov, Y. A.; Winey, J. M.; Gupta, Y. M. Spectroscopic Study of Shock-Induced Decomposition in Ammonium Perchlorate Single Crystals. *J. Phys. Chem. A* **2008**, *112*, 3947–3952.
- (18) Freeman, E. S.; Anderson, D. A.; Campisi, J. J. The Effects of X-Ray and Gamma Ray Irradiation on the Thermal Decomposition of Ammonium Perchlorate in the Solid State. *J. Phys. Chem.* **1960**, *64*, 1727–1732.
- (19) Levy, P. W.; Herley, P. J. Effects of Radiation on the Thermal Decomposition Induction Period in Ammonium Perchlorate and Other Pseudostable Materials. *J. Phys. Chem.* **1971**, *75*, 191–201.
- (20) Herley, P. J.; Wang, C. S.; Varsi, G.; Levy, P. W. Effect Of Fast Neutron, Gamma-Ray, And Combined Radiations On The Thermal Decomposition Of Ammonium Perchlorate Single Crystals. *J. Chem. Phys.* **1974**, *60*, 2430–2439.
- (21) Dedgaonkar, V. G.; Sarwade, D. B. Radiation Effects on Thermal Decomposition of Ammonium Perchlorate. *J. Radioanal. Nucl. Chem.* **1992**, *165*, 269–275.
- (22) Ivanov, E. Ju.; Khairtdinov, E. F.; Mulina, T. V. Photo-thermochemical Process in Ammonium Perchlorate Crystals: I. *J. Solid State Chem.* **1978**, *26*, 209–213.
- (23) Ivanov, E. Ju.; Khairtdinov, E. F.; Boldyrev, V. V. Photo-thermochemical Process in Ammonium Perchlorate Crystals: II. *J. Solid State Chem.* **1978**, *26*, 215–221.
- (24) Cole, T. Paramagnetic Defects in Irradiated NH_4ClO_4 . *J. Chem. Phys.* **1961**, *35*, 1169–1173.
- (25) Hyde, J. S.; Freeman, E. S. E.P.R. Observation of NH_3^+ Formed by X-Ray Irradiation of Ammonium Perchlorate Crystals. *J. Phys. Chem.* **1961**, *65*, 1636–1638.
- (26) Hegde, B. G.; Rastogi, A.; Damle, R.; Chandramani, R.; Bhat, S. V. An Electron Spin Resonance Study of ClO_3 Radicals in NH_4ClO_4 Single Crystals. *J. Phys.: Condens. Matter* **1997**, *9*, 3219–3226.
- (27) Janecka, J.; Fujimoto, M. ESR Studies of Restricted Random Motion of NH_3^+ Radicals in γ -Irradiated Ammonium Perchlorate Crystals. *J. Magn. Reson.* **1971**, *4*, 47–53.
- (28) Mishra, S. P.; Symons, M. C. R. Radiation Mechanisms Part 10—Comparison between the Effects of Fast Neutron Irradiation and ^{60}Co γ -Irradiation of a Range of Ionic and Non-Ionic Material. *J. Chem. Soc., Faraday Trans. 2* **1976**, *72*, 747–754.

- (29) Dedgaonkar, V. G.; Sarwade, D. B. Studies on Gamma Radiolysis of Microcrystalline Ammonium Perchlorate. *J. Radioanal. Nucl. Chem.* **1995**, *199*, 191–196.
- (30) Odian, G.; Acker, T.; Pletzke, T. γ -Radiolysis of Ammonium Perchlorate. *J. Phys. Chem.* **1965**, *69*, 2477–2479.
- (31) Maycock, J. N.; Pai Verneker, V. R. Ultraviolet Photon Induced Color Centers in Ammonium Perchlorate. *Solid State Commun.* **1969**, *7*, 979–981.
- (32) Ramaswamy, A. L.; Shin, H.; Armstrong, R. W.; Lee, C. H.; Sharma, J. Nanosecond and Picosecond Laser-Induced Cracking and Ignition of Single Crystals of Ammonium Perchlorate. *J. Mater. Sci.* **1996**, *31*, 6035–6042.
- (33) Yang, C. S.-C.; Brown, E. E.; Hommerich, U.; Jin, F.; Trivedi, S. B.; Samuels, A. C.; Snyder, A. P. Long-Wave, Infrared Laser-Induced Breakdown (LIBS) Spectroscopy Emissions from Energetic Materials. *Appl. Spectrosc.* **2012**, *66*, 1397–1402.
- (34) Yang, C. S.-C.; Brown, E. E.; Kumi-Barimah, E.; Hommerich, U.; Jin, F.; Jia, Y.; Trivedi, S.; D'Souza, A. I.; Decuir, E. A., Jr.; Wijewarnasuriya, P. S.; et al. Rapid Long-Wave Infrared Laser-Induced Breakdown Spectroscopy Measurements Using a Mercury-Cadmium-Telluride Linear Array Detection System. *Appl. Opt.* **2015**, *54*, 9695–9702.
- (35) Barber, M.; El-Issa, B. D.; Hinchliffe, A. SCF- $X\alpha$ Investigation of the Ionization Energies of ClO_4^- , SO_4^{2-} , and PO_4^{3-} . *J. Chem. Soc., Faraday Trans. 2* **1980**, *76*, 441–445.
- (36) Politzer, P.; Lane, P. Energetics of Ammonium Perchlorate Decomposition Steps. *J. Mol. Struct.: THEOCHEM* **1998**, *454*, 229–235.
- (37) Zhu, R. S.; Lin, M. C. A Computational Study on the Decomposition of NH_4ClO_4 : Comparison of the Gas-Phase and Condensed-Phase Results. *Chem. Phys. Lett.* **2006**, *431*, 272–277.
- (38) Zhu, W.; Wei, T.; Zhu, W.; Xiao, H. Comparative DFT Study of Crystalline Ammonium Perchlorate and Ammonium Dinitramide. *J. Phys. Chem. A* **2008**, *112*, 4688–4693.
- (39) Zhu, R. S.; Lin, M. C. Mechanism and Kinetics for Ammonium Perchlorate Sublimation: A First-principles Study. *J. Phys. Chem. C* **2008**, *112*, 14481–14485.
- (40) Radhakrishna, S.; Riggan, M.; Whippey, P. W.; Jacobs, P. W. M. Thermoluminescence of Irradiated Ammonium Perchlorate Crystals. *Can. J. Phys.* **1976**, *54*, 766–770.
- (41) Jones, B. M.; Kaiser, R. I. Application of Reflectron Time-of-Flight Mass Spectroscopy in the Analysis of Astrophysically Relevant Ices Exposed to Ionization Radiation: Methane (CH_4) and D4-Methane (CD_4) as a Case Study. *J. Phys. Chem. Lett.* **2013**, *4*, 1965–1971.
- (42) Maity, S.; Kaiser, R. I.; Jones, B. M. Infrared and Reflectron Time-of-Flight Mass Spectroscopic Study on the Synthesis of Glycolaldehyde in Methanol (CH_3OH) and Methanol-Carbon Monoxide ($\text{CH}_3\text{OH-CO}$) Ices Exposed to Ionization Radiation. *Faraday Discuss.* **2014**, *168*, 485–516.
- (43) Góbi, S.; Bergantini, A.; Kaiser, R. I. In Situ Detection of Chlorine Dioxide (ClO_2) in the Radiolysis of Perchlorates and Implications for the Stability of Organics on Mars. *Astrophys. J.* **2016**, *832*, 164.
- (44) Góbi, S.; Abplanalp, M. J.; Kaiser, R. I. Effect of Perchlorates on Electron Radiolysis of Glycine with Application to Mars. *Astrophys. J.* **2016**, *822*, 8.
- (45) Drouin, D.; Couture, A. R.; Joly, D.; Tastet, X.; Aimez, V.; Gauvin, R. CASINO V2.42—A Fast and Easy-To-Use Modeling Tool for Scanning Electron Microscopy and Microanalysis Users. *Scanning* **2007**, *29*, 92–101.
- (46) Frenklach, M.; Wang, H.; Rabinowitz, M. J. Optimization and Analysis of Large Chemical Kinetic Mechanisms Using the Solution Mapping Method—Combustion of Methane. *Prog. Energy Combust. Sci.* **1992**, *18*, 47–73.
- (47) Kim, Y. S.; Kaiser, R. I. Abiotic Formation of Carboxylic Acids (RCOOH) in Interstellar and Solar System Model Ices. *Astrophys. J.* **2010**, *725*, 1002–1010.
- (48) Maity, S.; Kaiser, R. I. Electron Irradiation of Carbon Disulfide – Oxygen Ices: Toward the Formation of Sulfur-Bearing Molecules in Interstellar Ices. *Astrophys. J.* **2013**, *773*, 184.
- (49) Kaiser, R. I.; Maity, S.; Jones, B. M. Infrared and Reflectron Time-of-Flight Mass Spectroscopic Analysis of Methane (CH_4)–Carbon Monoxide (CO) Ices Exposed to Ionization Radiation – Toward the Formation of Carbonyl Bearing Molecules in Extraterrestrial Ices. *Phys. Chem. Chem. Phys.* **2014**, *16*, 3399–3424.
- (50) Hilbig, R.; Wallenstein, R. Enhanced Production of Tunable VUV Radiation by Phase-Matched Frequency Tripling in Krypton and Xenon. *IEEE J. Quantum Electron.* **1981**, *17*, 1566–1573.
- (51) Miller, F. A.; Wilkins, C. H. Infrared Spectra and Characteristic Frequencies of Inorganic Ions. *Anal. Chem.* **1952**, *24*, 1253–1294.
- (52) Waddington, T. C. 881. Infrared Spectra, Structure, and Hydrogen-bonding in Ammonium Salts. *J. Chem. Soc.* **1958**, 4340–4344.
- (53) Van Rensburg, D. J. J.; Schutte, C. J. H. Low-Temperature Infrared and Raman Studies XI. The Vibrational Behaviour of Ammonium Perchlorate – Its Phase Changes and the Rotational Freedom of its Ions. *J. Mol. Struct.* **1972**, *11*, 229–239.
- (54) Turner, A. M.; Abplanalp, M. J.; Kaiser, R. I. Mechanistic Studies on the Radiolytic Decomposition of Perchlorates on the Martian Surface. *Astrophys. J.* **2016**, *820*, 127.
- (55) Góbi, S.; Förstel, M.; Maksyutenko, P.; Kaiser, R. I. A Reflectron Time-of-Flight Mass Spectrometric Study on the Degradation Pathways of Glycine on Mars in the Presence of Perchlorates and Ionizing Radiation. *Astrophys. J.* **2017**, *835*, 241.
- (56) Zheng, W.; Kaiser, R. I. An Infrared Spectroscopy Study of the Phase Transition in Solid Ammonia. *Chem. Phys. Lett.* **2007**, *440*, 229–234.
- (57) Fateley, W. G.; Bent, H. A.; Crawford, B., Jr. Infrared Spectra of the Frozen Oxides of Nitrogen. *J. Chem. Phys.* **1959**, *31*, 204–217.
- (58) Stirling, A.; Pápai, I.; Mink, J.; Salahub, D. Density Functional Study of Nitrogen Oxides. *J. Chem. Phys.* **1994**, *100*, 2910–2923.
- (59) Nightingale, R. E.; Wagner, E. L. The Vibrational Spectra and Structure of Solid Hydroxylamine and Deutero-Hydroxylamine. *J. Chem. Phys.* **1954**, *22*, 203–208.
- (60) Zheng, W.; Kaiser, R. I. Formation of Hydroxylamine (NH_2OH) in Electron-Irradiated Ammonia-Water Ices. *J. Phys. Chem. A* **2010**, *114*, 5251–5255.
- (61) Bernstein, M. P.; Sandford, S. A. Variations in the Strength of the Infrared Forbidden 2328.2 cm^{-1} Fundamental of Solid N_2 in Binary Mixtures. *Spectrochim. Acta, Part A* **1999**, *55*, 2455–2466.
- (62) Vandenbussche, B.; Ehrenfreund, P.; Boogert, A. C. A.; van Dishoeck, E. F.; Schutte, W. A.; Gerakines, P. A.; Chiar, J.; Tielens, A. G. G. M.; Keane, J.; Whittet, D. C. B.; et al. Constraints on the Abundance of Solid O_2 in Dense Clouds from ISO-SWS and Ground-based Observations. *Astron. Astrophys.* **1999**, *346*, L57–L60.
- (63) <http://webbook.nist.gov/cgi/cbook.cgi?ID=C10102440&Units=SI&Mask=200#Mass-Spec>.
- (64) Loch, R.; Hottmann, K.; Hagenow, G.; Denzer, W.; Baumgärtel, H. The Threshold Photoelectron Spectrum of NH_3 . *Chem. Phys. Lett.* **1992**, *190*, 124–129.
- (65) Lias, S. G.; Bartmess, J. E.; Liebman, J. F.; Holmes, J. L.; Levin, R. D.; Mallard, W. G. Gas-phase Ion and Neutral Thermochemistry. *J. Phys. Chem. Ref. Data, Suppl.* **1988**, *17*, 1–861.
- (66) Dibeler, V. H.; Walker, J. A.; Liston, S. K. Mass Spectrometric Study of Photoionization. VII. Nitrogen Dioxide and Nitrous Oxide. *J. Res. Natl. Bur. Stand., Sect. A* **1967**, *71A*, 371–378.
- (67) Schwell, M.; Jochims, H.-W.; Wassermann, B.; Rockland, U.; Flesch, R.; Rühl, E. Ionization Energies of ClO and Cl_2O_2 . *J. Phys. Chem.* **1996**, *100*, 10070–10075.
- (68) Flesch, R.; Rühl, E.; Hottmann, K.; Baumgärtel, H. Photo-absorption and Photoionization of Chlorine Dioxide. *J. Phys. Chem.* **1993**, *97*, 837–844.
- (69) Li, W.-K.; Lau, K.-C.; Ng, C. Y.; Baumgärtel, H.; Weitzel, K.-M. Gaussian-2 and Gaussian-3 Study of the Energetics and Structures of Cl_2O_n and Cl_2O_n^+ , $n = 1-7$. *J. Phys. Chem. A* **2000**, *104*, 3197–3203.

(70) Trickl, T.; Cromwell, E. F.; Lee, Y. T.; Kung, A. H. State-selective Ionization of Nitrogen in the $X^2\Sigma_g^+ \nu_+ = 0$ and $\nu_+ = 1$ states by two-color (1 + 1) photon excitation near threshold. *J. Chem. Phys.* **1989**, *91*, 6006–6012.

(71) Tonkyn, R. G.; Winniczek, J. W.; White, M. G. Rotationally Resolved Photoionization of O_2^+ Near Threshold. *Chem. Phys. Lett.* **1989**, *164*, 137–142.

(72) Turner, A. M.; Abplanalp, M. J.; Chen, S. Y.; Chen, Y. T.; Chang, A. H. H.; Kaiser, R. I. A Photoionization Mass Spectroscopic Study on the Formation of Phosphanes in Low Temperature Phosphine Ices. *Phys. Chem. Chem. Phys.* **2015**, *17*, 27281–27291.

(73) Sill, G.; Fink, U.; Ferraro, J. R. Absorption Coefficients of Solid NH_3 from 50 to 7000 cm^{-1} . *J. Opt. Soc. Am.* **1980**, *70*, 724–739.

(74) Saldyka, M.; Mielke, Z. Photodecomposition of Formohydroxamic Acid. Matrix Isolation FTIR and DFT Studies. *Phys. Chem. Chem. Phys.* **2003**, *5*, 4790–4797.

(75) Quinn, R. C.; Martucci, H. F. H.; Miller, S. R.; Bryson, C. E.; Grunthaner, F. J.; Grunthaner, P. J. Perchlorate Radiolysis on Mars and the Origin of Martian Soil Reactivity. *Astrobiology* **2013**, *13*, 515–520.

(76) Prince, L. A. Determination of Chloride, Hypochlorite, Chlorite, Chlorate, Perchlorate, and Chlorine Dioxide in Composite Mixtures. *Anal. Chem.* **1964**, *36*, 613–616.

(77) Wang, L.; Mebel, A. M.; Yang, X.; Wang, X. Ab Initio/RRKM Study of the $O(^1D) + NH_3$ Reaction: Prediction of Product Branching Ratios. *J. Phys. Chem. A* **2004**, *108*, 11644–11650.

(78) He, J.; Vidali, G.; Lemaire, J.-L.; Garrod, R. T. Formation of Hydroxylamine on Dust Grains via Ammonia Oxidation. *Astrophys. J.* **2015**, *799*, 49.

(79) Zheng, W.; Jewitt, D. C.; Osamura, Y.; Kaiser, R. I. Formation of Nitrogen and Hydrogen-Bearing Molecules in Solid Ammonia and Implications for Solar System and Interstellar Ices. *Astrophys. J.* **2008**, *674*, 1242–1250.

(80) Back, R. A. The Preparation, Properties and Reactions of Diimide. *Rev. Chem. Intermed.* **1984**, *5*, 293–323.